Hyperthermia system combined with a magnetic resonance imaging unit

J. Delannoy[a)]
Biomedical Engineering and Instrumentation Program, National Center for Research Resources and Radiation Oncology Branch/COP/DCT, National Cancer Institute, National Institutes of Health, Bethesda, Maryland 20892

D. LeBihan[b)]
Diagnostic Radiology Department, Warren Grant Magnuson Clinical Center, National Institutes of Health, Bethesda, Maryland 20892

D. I. Hoult and R. L. Levin
Biomedical Engineering and Instrumentation Program, National Center for Research Resources, National Institutes of Health, Bethesda, Maryland 20892

(Received 2 June 1989; accepted for publication 18 June 1990)

Magnetic resonance imaging (MRI) has recently been proposed as a method to monitor, noninvasively, temperature, blood flow, and cell metabolism during oncologic hyperthermia (HT). To heat and "image" simultaneously, it is necessary to combine a HT device and a MRI unit. As a demonstrative example of the problems associated with implementing such a system, a mini-annular phased array hyperthermia applicator was combined with a 0.5-T whole body MRI unit. With the aid of filters, baluns, and switches, the HT applicator and the MRI unit were made compatible. The overall system was tested using a muscle-equivalent, cylindrically shaped polyacrylamide gel phantom. No interference between the HT device and the MRI unit was observed. Noninvasive temperature images, with a resolution better than 1 °C/cm, were obtained from images of molecular diffusion recorded before and during heating.

Key words: hyperthermia, magnetic resonance imaging, molecular diffusion, therapeutic radiology technology, temperature imaging

I. INTRODUCTION

Many clinical studies have shown the effectiveness of hyperthermia (HT) as an adjuctive treatment for malignancies, when used in combination with radiotherapy or chemotherapy.[1-3] Efficacy requires that temperatures within tumor(s) remain above 43 °C for 30 to 60 min, while safety considerations limit temperatures in normal tissures to below 43 °C. It is therefore necessary to control the temperature in real time throughout the heated volume to better than 1°C. Over the past several years, hyperthermia devices have been improved significantly so that it is now possible to focus the energy into a given region of the body.[1,4] Despite these advances the lack of adequate temperature control limits the usefulness of such devices. Temperatures can be measured with good accuracy by invasive means, such as thermocouples, thermistors or fiber-optic probes, but only regions in close proximity to the probes are monitored.[5,6] Furthermore, probe insertion may be painful and hazardous. Various noninvasive methods have previously been proposed to monitor temperature during hyperthermia. However, it is difficult to achieve deep measurements with microwave radiometry and infrared thermography, while ultrasound, computed tomography (CT), and active microwave techniques lack the required accuracy or resolution.

Magnetic resonance imaging (MRI) is a noninvasive and nonionizing technique which produces anatomical images in any orientation. Its use as a means to "map" temperature was suggested several years ago.[7-9] Unfortunately, these attempts were unsuccessful because the parameter used, namely, the relaxation time $T1$, is difficult to measure accurately by MRI and changes in proton relaxation may have a complex relation with temperature.[10,11] On the other hand, there is a well-known relationship between molecular diffusion that can be measured and imaged with MRI and temperature.[12] Based on this fact, it has recently been shown that temperature imaging in phantoms could be obtained with good accuracy and resolution (better than 0.5 °C/cm) using magnetic resonance imaging of molecular diffusion.[13] Furthermore, the same technique could be used to evaluate tissue perfusion,[14] the dominant physiological mechanism for removing heat during hyperthermia,[15-17] while MR spectroscopy possibly could be used to monitor tumor metabolism.[18] Therefore, MRI could be a very effective tool for the control of HT treatments.

To use MRI to monitor hyperthermia, however, it is necessary to combine a hyperthermia device with a MRI unit. This is not *a priori* trivial since each device might be functionally disturbed, if not damaged, by the presence of the other. The purpose of this study is to present the solutions which we have adopted to overcome this technical challenge.

II. COMBINING HYPERTHERMIA AND MRI

A. Hyperthermia systems

Heating is produced, in most cases, by depositing ultrasonic or electromagnetic energy directly into the tissues of interest. For the latter case, energy deposition in a given

 0094-2405/90/050855-06$01.20

location depends on the local electric field strength and on the tissures' local dielectric characteristics. Using a single, plane-wave, external, electromagnetic applicator, energy deposition usually is maximal at the skin surface and decreases more or less exponentially with depth. To reverse this trend, various types of multiple applicator systems have been proposed.[1,4,19–22] These devices rely upon the phase and amplitude interaction of the field emanating from each of their applicators to minimize energy deposition in the superficial layers and to maximize energy deposition in the deep regions. However, the resulting temperature distribution depends not only upon the energy deposition pattern but also upon the thermal clearance, mainly via perfusion, within the heated tissures.[15–17] These factors make it difficult to predict the temperature distribution that will be achieved within the region to be treated so that temperature mapping is essential.

B. Compatibility problems

Compatibility problems may be expected to arise mainly from the interactions of the strong magnetic field and the radiofrequency fields used by the MR system with the applicator of the HT system. The hyperthermia device must be able to work under such conditions and must be also physically compatible; that is, it must fit inside the MR transmitting and receiving coils. The most critical challenge, however, is to assure the correct operation of the MR unit in the presence of the HT device. The main magnetic field of the MR unit should not be distorted by the presence of any ferromagnetic parts. In addition, the radiofrequency field seen by nuclei should not be perturbed by the presence of the HT device. The HT device must also not include large metallic parts that could be the origin of eddy currents when the MRI gradient coils are switched. Finally, and perhaps most important, the MR signal derived from the nuclei, which is of the order of nanowatts, must be purged of any radiofrequency pollution emanating from the hyperthermia applicators which are operating in a close frequency range at the level of several hundred watts. Current MRI systems use frequencies from 4 to 85 MHz, while frequencies used with the chosen hyperthermia applicator are from 100 to 200 MHz. These frequencies might appear far enough from each other not to induce any interference; but since high power is required by the HT applicator, one should fear some leakage out of the expected frequency range. Note that the MRI preamplifier was designed to handle microvolt signals and would be damaged by any large signal.

III. MATERIAL AND METHODS

We used a whole body MRI system (Magniscan 5000, Thomson-CGR) working at 21 MHz with a 0.5-T magnetic field in combination with a mini-annular phased array (MAPA) radio-frequency HT applicator, which had previously been designed to treat limb tumors.[19–22]

The MAPA frame was originally 30 cm in outer diameter and 30 cm in length. A new smaller MAPA was built to fit within the MRI system's head coil. While its length was kept at 30 cm, its outer diameter was reduced to 25 cm (see Fig. 1). The MAPA's frame is a thin wall, 0.5-cm-thick Plexiglas® cylinder. Four axially oriented, double, trapezoidally shaped dipole antennas are evenly spaced on the frame's internal circumference. The antennas are constructed from very thin (30 μm) copper foil in order to minimize eddy currents during gradient switching. All ferromagnetic components such as bolts, coaxial wires, power divider and connectors, contained in the original design were eliminated. Typically, the dipoles of the MAPA are activated at a single frequency with signals of equal amplitude and phase in order to maximize the energy deposition at the center of the applicator.[19–21] However, it is possible to vary the MAPA's specific absorption rate (SAR) pattern by activating each dipole using rf signals differing in frequency, phase and/or amplitude.[22] The MAPA can also operate anywhere in the frequency range of approximately 100 to 200 MHz. A single working frequency of 168 MHz (i.e., eight times the MR frequency) was chosen to simplify construction of the appropriate baluns and filters. To maximize the coupling between the MAPA and the extremity being heated (i.e., to achieve a good "match") and to enable surface cooling, a fluid-filled deformable plastic bolus is used to fill the space between the dipole arrays and the limb.

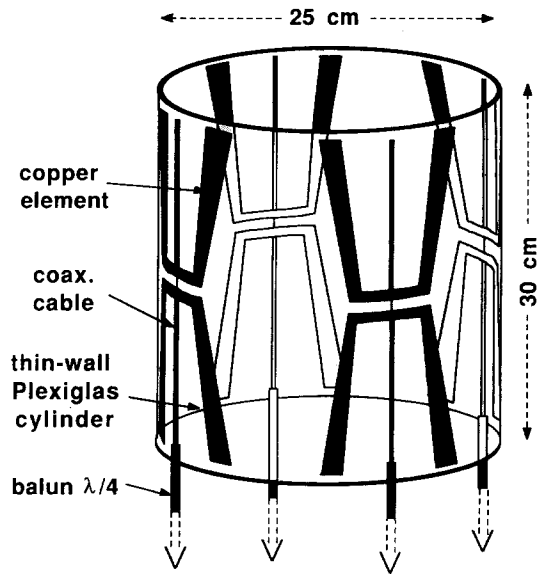

FIG. 1. New MAPA applicator. A new MAPA applicator was designed to be compatible with the whole body MRI unit. The MAPA is 25 cm in diameter and fits within the MRI head coil. Its length is 30 cm. The frame consists of a thin wall (0.5-cm-thick) Plexiglas® cylinder. Four, axially oriented, trapezoidal double dipoles antennas are evenly spaced on the frame's internal circumference. The antennas are constructed from very thin (30 μm) copper film to minimize eddy currents during gradient switching. All ferromagnetic components of the original design were also eliminated. Typically, the dipoles of the MAPA are activated at a single frequency with signals of equal amplitude and phase in order to maximize the energy deposition at the center of the applicator. To maximize the coupling between the MAPA and the extremity being heated and to enable surface cooling, a fluid-filled bolus is used to fill the space between the dipole arrays and the limb.

Each antenna is supplied with rf power via a 50-Ω nonferromagnetic coaxial cable (RG-58) balanced with a 168-

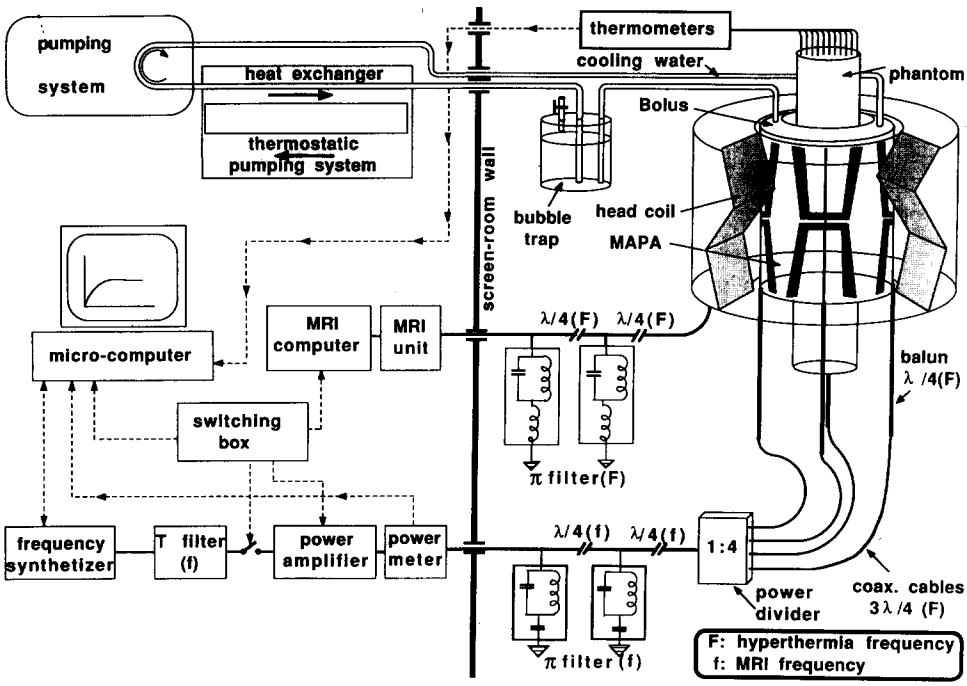

FIG. 2. General diagram of the combined HT–MRI system. The right-hand side of the drawing illustrates the components which reside inside the MRI screen room. The MAPA is situated inside the head coil of the MRI unit. It is activated with rf power via baluns, a power divider, and a π filter. A π filter is also used on the MRI coil to protect the MRI receiver. A switching box serves as the master clock for the heating/imaging time sharing process. Invasive temperature measurements are recorded within the phantom using thermocouples whose readings are manually logged or fiber optic probes whose readings are automatically logged by a microcomputer system.

MHz, $\lambda/4$, bazooka-type balun which is linked to a 1:4 power divider via a $3\lambda/4$ (at 168 MHz) line (see Fig. 2). The baluns are axially oriented. However, to prevent any capacitive interaction with the dipole antennas, the baluns are not physically attached to the MAPA at the center of each dipole array. Rather, they are connected to the centers by 15-cm lengths of RG-58 coaxial cable, additional 15-cm pieces being attached on the other sides of the dipoles to ensure symmetry (see Fig. 1). The power divider was connected by a high-power, low-loss 50-Ω coaxial cable (Belden 9913, RG-8 type), via a grounded bulkhead fitting through the screen room wall to a 1-kW cw broadband amplifier (Instruments for Industry model 406) located outside the screen room. This 50-Ω power line included a π section filter, located between the MAPA and the screen room wall. The filter consisted of a $\lambda/4$ (at 21 MHz) line at each end of which were two identical resonant circuits to "ground". Each circuit consisted of a parallel resonating circuit adjusted for 168 MHz combined with a series circuit resonating at 21 MHz. The rest of the line between the MAPA and the HT amplifier had no particular prescribed length. The π filter thus rejected 21 MHz with no significant attenuation at 168 MHz, thereby effectively preventing the MRI rf pulses from damaging the HT electronic equipment and ensuring that no interference reached the MRI receiver. The HT amplifier was driven by a solid-state signal generator (Fluke model 6060A). Forward and reflected powers were monitored by a 438A Hewlett-Packard bidirectional power meter with two 8482A power sensors using a high-power, dual-directional coupler (Amplifier Research model DC2000). All equipment for the HT system was positioned outside the screen room as far from the magnet as possible in order to minimize any effect from the fringe magnetic field of the MR unit. The large electric fields generated by the MAPA can capacitively couple to the MRI system's head coil. Thus the MRI receiver had to be protected with a π filter, similar to that described above, that rejected 168 MHz while giving negligible attenuation at 21 MHz. Although this protected the MRI preamplifier against damage, it could still be saturated during heating, making imaging impossible. Since further filtering would have degraded the MR unit's signal-to-noise ratio, it was therefore necessary for us to heat and image in a time sharing manner. A blanking circuit on the HT rf power amplifier was used to deactivate the power supply of the last stage of the IFI unit and thereby block any rf noise issuing therefrom. In addition, a pin-diode switch between the signal generator and the amplifier was used. A T filter (-40 dB) was also inserted between the rf generator and the amplifier to stop passively any 21-MHz signal (emitted inadvertently from the signal generator) from damaging the MR unit's preamplifier.

To control the heating/imaging time-sharing process, a switch box was constructed. For the MRI system, this switching unit was connected to the "cardiac gating" input normally used to synchronize imaging with electrocardiographic (ECG) signals. For the HT system, the switching unit was connected to both the pin-diode switch located between the signal generator and the amplifier and to the blanking circuit of the amplifier. To avoid "blanking" the rf amplifier in the presence of an rf input signal, the amplifier was switched on 5 ms before, and off 5 ms after, the pin diodes. Imaging was performed between the heating periods. The total heating/imaging cycle was set to a 1-s repetition time (TR), which corresponded to a 700-ms heating period during the "dead time" of each MRI acquisition cycle. In this way imaging and heating could be achieved efficiently with no time wasted.

The HT system was controlled by a PC/AT clone computer which was digitally connected to (i) the rf signal generator and rf power meter via an IEEE-488 interface and (ii)

the rf amplifier via four input and four output digital lines. The keyboard and monitor of the PC/AT were extended to the MRI console room by a serial communication link so that both the HT and MR systems could be monitored conveniently.

A special plastic support was made to fasten the MAPA rigidly to the MRI's mobile patient support table and the table's guide track (Fig. 3). To minimize motion artifacts due to mechanical vibrations induced by the gradient coils, the MAPA was not permitted to make contact with any other part of the MRI unit.

The MAPA's bolus fluid was supplied via a closed circuit pumping system which included (i) a pulse-free, rf noise-free (asynchronous motor), centrifugal pump, (i) a tube-in-shell heat exchanger, (iii) a bubble trap, and (iv) 1.6-cm (5/8-in.) i.d. reinforced PVC tubing. A thermostatically regulated pumping system situated outside the screen room was used to adjust the bolus coolant temperature via the heat exchanger located within the screen room. Water flow through the screen room wall was achieved by passing the PVC water lines through two waveguides (20 cm in length, 3 cm in diameter) located in the screen room wall. Since MRI is very sensitive to overall movements of the object to be imaged, a paramagnetic solution of manganese chloride (1 mM/l) was used instead of distilled water as the bolus fluid. The manganese chloride did not affect the dielectric properties of the bolus fluid sufficiently to modify the MAPA's power deposition pattern, but it did decrease dramatically the bolus fluid's relaxation time so that, with the appropriate imaging sequence, the signal coming from the bolus was negligible compared to that coming from the phantom. Because the bolus fluid was not visible in the diffusion and derived-temperature images, it could be circulated during imaging.

The complete HT–MRI system was tested using a leg phantom. This phantom consisted of a 12-cm-i.d., 60-cm-long thin-wall (0.5-cm) Plexiglas® tube filled with polyacrylamide gel (92.5% water) doped with copper sulfate (5 mM/l) so that the relaxation times were close to those expected *in vivo*. Eleven 16-gal. Teflon® catheters (2-mm o.d.) were also placed longitudinally, 1 cm apart, within the gel, permitting us to insert thermal probes.

Invasive temperature measurements were made using either fiber optic probes or thermocouples. The fiber optic system consisted of a Luxtron model 3000 fluoroptic 8 channel system, which was located inside the screen room, and 8 Luxtron MPM 0.7-mm-o.d. single-point thermal probes. By means of a fiber optic RS 232 link though the screen room wall, data from the Luxtron unit were logged in real time by the PC/AT computer system located outside the screen room. The thermocouple system consisted of a digital thermometer (Bailey Sensortek model BAT-12) and 11 miniature (0.23-mm o.d.) Teflon® coated probes having a very short time constant (0.1 s). Because these thermocouples are sensitive to rf fields, thermocouple temperatures were recorded manually during short periods when both the HT and MR were quiescent.

To test our ability to image through the MAPA, an initial series of tests was performed in the absence of any HT rf power using sequences that were sensitized to rf and magnetic field inhomogeneities (e.g., gradient echo). Later, hyperthermia sessions were performed on phantoms using a 1-Hz, 70% duty cycle (e.g., HT heating for 700 ms and MR imaging for 300 ms every second). During these simulated hyperthermia sessions, the MAPA cooling system was adjusted to obtain a temperature of ≈ 15 °C within the bolus. The phantom was initially heated with 300 W of rf power for 30 min. This produced a temperature gradient of ≈ 3 °C within the phantom (e.g. ≈ 33 °C at the center of the phantom and ≈ 20 °C at the most peripheral catheter). The HT rf power was then reduced to ≈ 100 W to maintain a steady state. After an additional ≈ 15 min, a diffusion image was recorded over a time period of 7 min. A temperature image was then computed immediately using the MRI's processing system which consists of a DEC VAX-11/730 computer coupled to an MSP-3000 array processor.

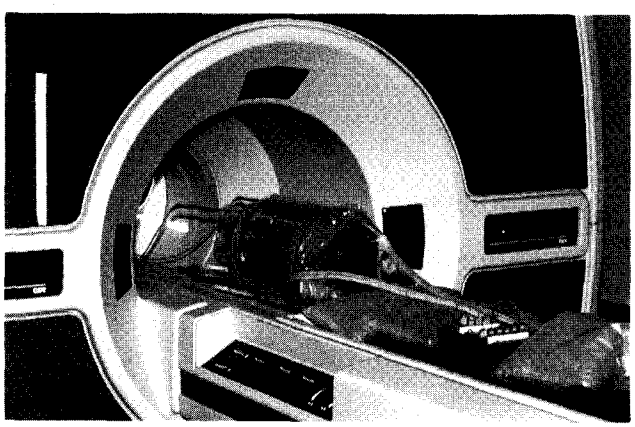

FIG. 3. MAPA applicator poised to be inserted into the tunnel of the MRI unit. The MAPA is attached to a special plastic support which is rigidly fastened to both the mobile patient support table of the MRI unit and the table's guide track. The MAPA has no other mechanical contact with the MRI unit. A doped polyacrylamide phantom is placed approximately in the middle of the MAPA while a fluid-filled bolus is used to couple the MAPA to the phantom.

IV. RESULTS

A. Compatibility of MAPA and MRI systems

Images were first recorded using pulse sequences sensitized to rf and magnetic field inhomogeneities (e.g., gradient echo). No artifacts or other distortions were found (see Fig. 4). We therefore concluded that the physical presence of the MAPA did not interfere with the normal functioning of the MRI system. However, before beginning the heating studies, several additional compatibility tests were performed. First, the "cross-talk" between the two systems was found to be < 600 mV at the MRI receiver input when the MAPA was being activated with 1-kW cw. Second, the presence of both the minature thermocouples and the fiber optic probes was not detectable in any of the images. Also, these particular sensors and their electronic control units produced no artifacts.

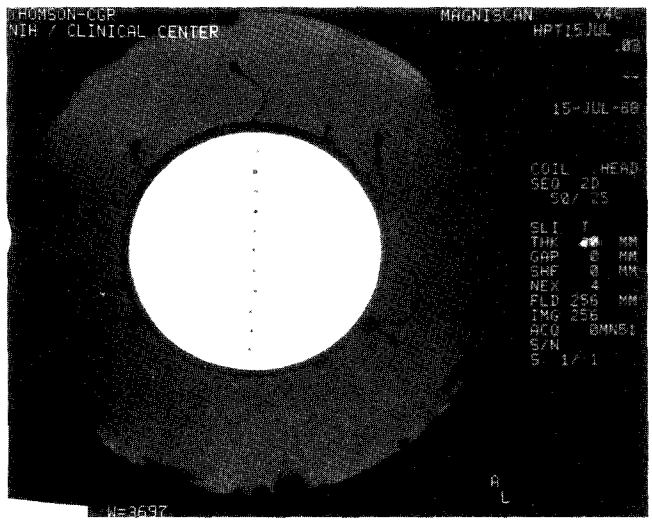

FIG. 4. MR gradient echo image of the phantom with the MAPA and all supporting baluns, power divider, and filters in place. The bolus, which consists of a PVC bag of a paramagnetic solution of manganese chloride (1 mM/l) and water, is almost invisible. The polyacrylamide phantom is clearer because it contains copper sulfate. Temperature measurement catheters are also visible. The MAPA itself is not visible because it does not contain any water. There are no artifacts nor distortions due to the presence of the MAPA.

B. Temperature imaging during hyperthermia

A temperature image computed in quasi real time from steady-state diffusion images recorded before and during a heating is shown in Fig. 5. The pixel size is 2×2 mm (128×128 pixels) and the slice thickness is 20 mm. Brightness is directly proportional to temperature. Consequently, it is possible to read directly the temperature on the MRI console by moving the cursor to any location within the picture or to plot a thermal profile computed from a selected region of interest (ROI). Also, because the phantom was not centered exactly within the MAPA, it can be seen that the point of maximum energy deposition (i.e., the "hot spot") was not exactly at the center of the phantom but shifted slightly downwards. It can also be noted that the manganese chloride solution used for the circulating coolant makes the bolus virtually transparent.

To avoid catheter zones where no MR signal was recorded, temperature profiles were recorded from ROI's 1 cm wide and 11 cm long on both sides of the catheter plane. The mean of these measurements, recorded symmetrically every 5 mm along the two ROI profiles, together with the temperatures recorded by the probes within the catheters, which were spaced 1 cm apart, can be seen in Fig. 6. The correlations between our noninvasive and invasive temperature measurements are good and confirm our previously reported preliminary results.[13]

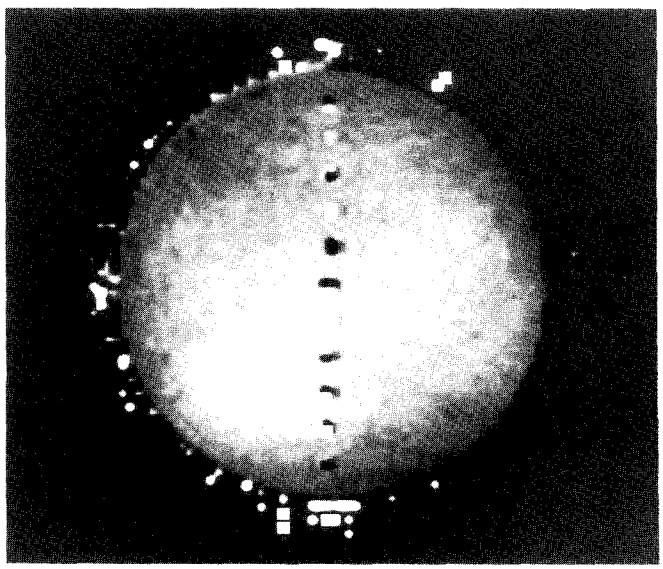

FIG. 5. Temperature image obtained during hyperthermia using a homogeneous phantom. This is a temperature image computed using the MRI unit's computer system from diffusion images recorded before and during heating. The acquisition time is 7 min. It is possible to read directly the temperature on the MRI console by moving the cursor to any location within the picture or to plot a thermal profile computed from a selected ROI. High-intensity points located in the vicinity of the catheters and the phantom's shell are calculation artifacts or no signal zones.

V. DISCUSSION

The feasibility of successfully image and measure temperature using MRI of diffusion is expected to be a "better parameter" than $T1$ for temperature measurements because its sensitivity to temperature change is greater. Furthermore, measuring $T1$ with MR imaging techniques is long and difficult, and $T1$ is dependent on many other parameters than temperature. On the contrary, the relationship between temperature and diffusion that reflect brownian motion is direct. Diffusion imaging is virtually insensitive to artifacts related to rf inhomogeneities[14] which is not the case of $T1$ imaging.

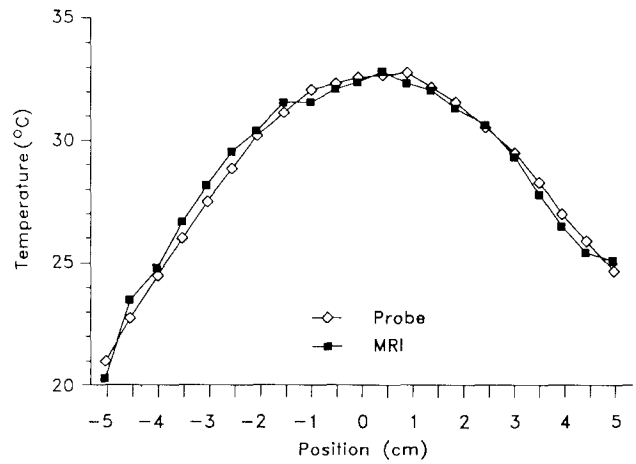

FIG. 6. Correlation between MRI noninvasive temperature measurements and standard probe invasive gemperature measurements. Standard thermal probes were used to record a profile within the catheter plane (unfilled boxes). Filled boxes show the temperature measurements done by averaging two regions of interests (ROIs) placed on either side of the catheter plane. The resolution is better than 1 °C with a 10-mm spatial resolution.

On the basis of this study, we believe that it is possible to combine a HT system with a MR system to monitor temperature non-invasively during clinical hyperthermia. Furthermore, because high-resolution standard MR anatomical images are readily available and can be superimposed on the temperature images, this technique should greatly facilitate the localization of the heating pattern within tumors so that normal tissues can be spared the deleterious effects associated with high temperatures. In addition to monitoring temperature during hyperthermia, MRI could potentially be used for monitoring perfusion[13,14] and various metabolic processes during heating.[18]

Although our results using muscle equivalent phantoms still need to be confirmed *in vivo*, our measured temperature resolution of better than 1 °C and spatial resolution of 10 mm should be adequate for clinical purposes. The current time scale of 7 min for the acquisition of a temperature image, however, limits us to monitoring quasi steady-state situations. We believe that this limitation can be overcome by implementing fast imaging techniques such as steady-state free precession[23] and echo-planar imaging.[24] These two imaging methods have recently yielded diffusion images and therefore should permit real time noninvasive temperature monitoring. Also, other types of electromagnetic or ultrasonic applicators can be used with MRI. All will face similar compatibility problems.

The major drawbacks of using magnetic resonance techniques to monitor noninvasively temperature and other physiological processes during clinical hyperthermia are that (i) despite the continuing increase in the number of MRI units, MRI procedures are expensive and HT treatments require 1 to 2 h long periods, and (ii) current methods for temperature imaging only measure changes in temperature as opposed to the actual temperature.[13] The first drawback is a medical economics issue whose resolution depends upon the efficacy of using MRI for monitoring temperature and other physiological processes noninvasively throughout the treatment area as opposed to using probes for monitoring temperature and/or perfusion invasively at a few preselected sites within the treatment area. The second drawback can be circumvented by either one or two methods. First, either the volume to be treated can be assumed to be at a relatively known homogeneous temperature, a reasonable assumption for abdominal or pelvic situations; or the volume to be treated can be brought to a relatively known homogeneous temperature by surrounding it with a fluid-filled bolus maintaned at normal body temperature. This is a reasonable assumption for limbs. Second, invasive probes at a few preselected sites in different types of tissues can be used to validate the MRI readings during the actual HT session.

[a] Present Address: Sonotron HITACHI, 1 rue de Terre Neuve, Miniparc du verger, Z. A. de Courtaboeuf, 91967 Les Ulis, France.

[b] Address reprint requests to: Dr. D. Le Bihan, Diagnostic Radiology Department, Bldg 10, Rm 1C660, National Institutes of Health, Bethesda, Maryland 20892, (301) 496-7700.

[1] G. M. Hahn, *Hyperthermia and Cancer*, 2nd ed. (Plenum, New York, 1982).

[2] R. S. Scott, R. J. Johnson, D. V. Story, and L. Clay, "Local Hyperthermia in combination with definitive radiotherapy: increased tumor clearance, reduced recurrence rate in extended follow-up," Int. J. Rad. Onc. Biol. Phys. **10**, 2219–2123 (1984).

[3] C. E. Lindholm, P. Kjellen, P. Nilsson, T. Landberg, B. Person, "Microwave-induced hyperthermia and radiotherapy in human superficial tumors: clinical results with a comparative study of combined treatment versus radiotherapy alone," Rec. Res. in Cancer Res. **107**, 152–156 (1988).

[4] *Physics and Technology of Hyperthermia*, edited by S. B. Field and C. Franconi (Martinus Nijhoff, Dordrecht, 1987).

[5] F. A. Gibbs, M. D. Sapozink, and J. R. Stewart, "Clinical Thermal Dosimetry: Why and How?," *Hyperthermic Oncology*, 1st ed., edited by J. Overgaard, (Taylor and Francis, Philadelphia, 1984), Vol. 2, pp. 155–167.

[6] T. C. Cetas, "Will thermometric tomography become practical for hyperthermia treatment monitoring?" Cancer Res. (suppl) **44**, 4805–4808 (1984).

[7] D. L. Parker, V. Smith, P. Sheldon, L. E. Crooks, and L. Fussel, "Temperature distribution measurements in two-dimensional NMR imaging," Med. Phys. **10**, 321–325 (1983).

[8] R. J. Dickinson, A. S. Hall, A. J. Hind, I. R. Young, "Measurement of changes in tissue temperature using MR imaging," J. Comput. Assist Tomogr. **10**, 468–472 (1986).

[9] H. Tanaka, K. Eno, H. Kato, T. Ishida, "Possible application of noninvasive thermometry for hyperthermia using NMR," Nippon Acta Radiol. **41**, 897–899 (1981).

[10] C. J. Lewa and Z. Majewska, "Temperature relationships of proton spin-lattice relaxation time $T1$ in biological tissues," Bull. Cancer (Paris) **67**, 525–530 (1980).

[11] F. A. Jolesz, A. R. Bleier, P. Jakab, P. W. Ruenzel, K. Huttl, and G. J. Jako, "MR imaging of laser-tissue interactions," Radiology **168**, 249–253 (1988).

[12] J. H. Simpson and H. Y. Carr, "Diffusion and nuclear spin relaxation in water," Phys. Rev. **111**, 1201–1202 (1958).

[13] D. Le Bihan, J. Delannoy, and R. L. Levin, "Non-invasive temperature mapping using magnetic resonance imaging of molecular diffusion: application to hyperthermia," Radiology **171**, 853–857 (1989).

[14] D. Le Bihan, E. Breton, D. Lallemand, M. L. Aubin, J. Vignaud, and M. Laval-Jeantet, "Separation of diffusion and perfusion intravoxel incoherent motion MR imaging," Radiology **168**, 497–505 (1988).

[15] G. M. Hahn, "Blood flow in *Physics and Technology of Hyperthermia*, 1st ed., edited by S. B. Field and C. Franconi (Martinus Nijhoff, Boston, 1987), pp. 441–447.

[16] *Heat Transfer in Medicine and Biology*, edited by A. Shitzer and R. C. Eberhart, (Plenum, New York, 1985).

[17] J. Delannoy, G. Giaux, A. Dittmar, W. H. Newman, G. Delhomme, and D. Delvallee, "Measurements of effective thermal conductivity during hyperthermia: a comparison of experimental and clinical results," Int. J. Hyperthermia (in press).

[18] P. W. Vaupel, P. G. Okunieff, and L. J. Neuringer, "Hyperthermia induced changes in tumor pH and energy status level evaluated by *in vivo* 31P nuclear magnetic resonance spectroscopy," in *Proceedings of the Society of Magnetic Resonance in Medicine* (Society of Magnetic Resonance in Medicine, Berkeley, 1988), Vol. 1, p. 412.

[19] P. F. Turner, "Mini-annular phased array for limb hyperthermia," IEEE Trans Microwave Theory Tech. **34**, 508–513 (1986).

[20] J-L. Guerquin-Kern, M. J. Hagmann, and R. L. Levin, "Experimental characterization of the mini-annular phased array as a hyperthermia applicator," Med. Phys. **14**, 674–680 (1987).

[21] C. Charny, J-L. Guerquin-Kern, M. J. Hagmann, S. W. Levin, E. E. Lack, W. F. Sindelar, A. Zabell, E. J. Glatstein, and R. L. Levin, "Human leg heating using a MAPA," Med. Phys. **13**, 449–456 (1986).

[22] C. Charny, J-L. Guerquin-Kern, and R. L. Levin, "Energy deposition patterns in amputated human lower legs heated with a Mini-Annular Phased Array," Med. Phys. **15**, 17–23 (1988).

[23] D. Le Bihan, "Intravoxel incoherent motion imaging using steady-state free precession," Magn. Reson. Med. **7**, 346–351 (1988).

[24] R. Turner and D. LeBihan, "Single-shot diffusion imaging at 2.0 Tesla," J. Mag. Res. **86**, 445–452 (1990).